Remote Sensing of Urban Environments - the Beijing Case Study

Definition and key parameters

Remote sensing data are used together with demographic parameters to characterize and monitor urban environments. For urban remote sensing, key measurements include night-light (NL) from visible-near infrared sensors, multispectral signatures having different spectral mixing (SM) for different land cover categories, and high-resolution radar backscatter (σ_0) obtained from scatterometer data with the Dense Sampling Method (DSM). NL is defined as the light occurred in areas lit by anthropogenic sources at nighttimes. SM is a composition of signatures from multiple channels with different electromagnetic wavelengths corresponding to blue, green, and red in the visible light range, and also to parts of the near infrared. DSM σ_0 in an urban area represents the radar cross section from ensembles of targets such as houses, buildings, factories, and other man-made infrastructures on land surface. Associated with σ_0 for each target ensemble, an index of variability (IV) is defined as $(1 + \delta/\sigma_0)$ in decibel, where δ is the standard deviation. Among the critical datasets to describe social and economic patterns are population and road network. The residential population (P_r) is defined as the population counted in each administrative unit. The ambient population (P_a) represents the number of daily averaged people located in each gridded pixel. Road network data are available in many formats from various sources that are routinely updated. These parameters will be further described in detail in the sections below. In this chapter, Beijing in China is used to illustrate the general points.

Urban landscape

Remote sensing technology offers some unique images and data of the urban landscape. Much of this chapter explains the contributions that remotely sensed data make independent of other data sets. In this section, we also describe the contribution of such data when used in combination with demographic and socioeconomic data. Particularly where the latter types of data are lacking, the combination of data sources may be especially powerful for identifying and monitoring the physical and human urban landscape.

Cities exist largely because people and capital become more productive when they cluster close together. Yet, for urban growth to be beneficial, urban policy making must reconcile three main objectives: economic growth, equity among the population, and environmental sustainability. Additionally, to achieve these objectives, policy makers must facilitate mobility which requires setting aside sufficient land for public and private forms of transport. Maintaining environmental sustainability also requires good institutions and enforcement for making smart land-use decisions that encourage efficient transport and a safe built environment. Moreover, climate change and potential exacerbation of disasters such as flood and drought extremes are major factors in long-term sustainable urban planning.

Designing the right policy instruments to help make urban growth productive and sustainable requires up-to-date information. However, most cities do not have the capacity to maintain up-to-date land registries and land-use maps at a fine scale. Population and housing censuses provide some information about who lives where and the characteristics of the dwellings and residents, but are typically collected only once per decade. Information on individual parcels of land (e.g., through tax records) is even sparser in most countries. Even where such statistical systems are introduced, they lack a retrospective perspective. Remote sensing data can help fill these data gaps and improve urban management, planning, and monitoring.

Here, Beijing is used as a case study. This city represents an example of rapid urban growth in an emerging economy. Since the 1980s, China implemented containment strategies to restrict or guide urban growth. In the face of double-digit economic growth concentrated in the urban areas in Eastern China, Beijing and other cities have nevertheless struggled to address the needs for economic growth, rapid motorization driven by rapid income growth, huge demand for housing from migrants, and wealth-driven demand for larger floor space. Between 1990 and 2008 its population grew from 10.8 million to 17 million on a land area of 16,410 km^2. Population is coarsely allocated into administrative units (Figure 1), which are arbitrarily defined with boundaries determined by obscure political processes. Further compounding the

uncertainty, these are official figures and do not include the “floating” population – migrants who do not hold official, Hukou, registration cards (Chengrong et al., 2008; Yeh and Xu 2009). Because the floating population is hard to capture through the official census, it is important to consider alternative means for identifying areas of urban change.

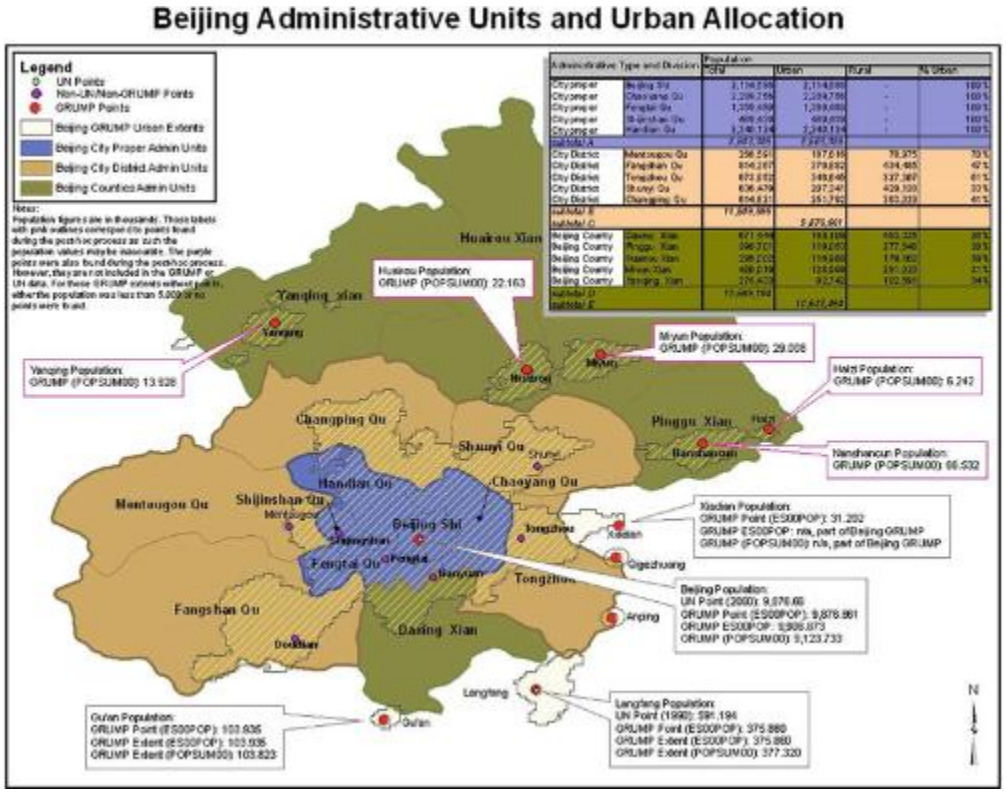

Figure 1 Beijing administrative unit and urban allocation. NL9495 extent is denoted by the hatched areas. Blue, brown, and green areas indicate the administrative areas for Beijing city proper, city district, and county, respectively. Depending on how one defines the urban contours of Beijing, using administrative data alone produces more than one estimate of population within urban Beijing. The dots in the figure represent settlement points, i.e., aspatial representations of urban areas. The United Nations’ World Urbanization Prospects and associated database identifies two settlements (green dots inside red dots at Beijing Shi and Langfang) in the Beijing region. GRUMP identifies 11 settlements (red dots) in the same area. The overlay of the NL9495 extent with administrative and point data help to reveal locations missing possible point representation; those places (purple dots) were identified ex-post-facto after GRUMP. For many GRUMP settlements, it is possible to generate a series of possible comparative population estimates, as noted in the call out boxes. In GRUMP, NL9495 data give an urban space to the point that the UN identifies as Beijing, and further combine space between administrative areas. In Beijing county, the NL data identify urban areas that would otherwise be undefined spatially within the county

Remote sensing can help generate relevant information for policy analysis and research (Liu et al. 2002; Angel et al. 2007). By coupling population data with remote sensing data, it is possible to gain another view of the urban form. The combination of remote sensing and demographic data is a powerful tool for detecting changes that may occur between censuses. In countries with restrictive data-use policies on finely resolved census-type data, remote sensing data may also provide a means to fill-in where a census cannot; such is the case of Beijing. Uninhibited by administrative or political constraints, remote sensing data provide useful urban information where other data sources are restricted.

Remote sensing approaches

Satellite remote sensors, useful for observations of urban environments, operate at frequencies across the electromagnetic spectrum from visible to microwave. In particular, this chapter presents results derived from Optical Line Scanner, Landsat, and QuikSCAT satellite data. These datasets have been successfully applied to urban studies.

Night-light

Global NL data, acquired by the Defense Meteorological Satellite Program (DMSP) Operational Line Scanner (OLS), have been used as a proxy indicator of urban areas (Elvidge et al. 1997, 2001, 2004; Sutton et al. 1997, 2001; Owen et al. 1998; Balk et al. 2006). The DMSP OLS was designed to collect global cloud imagery using a pair of broad spectral bands placed in the visible and thermal. The DMSP satellites are flown in polar orbits and each collects 14 orbits per day. With a 3,000 km swath width, each OLS is capable of collecting a complete set of images of the Earth twice a day. At night, the visible band signal is intensified with a photomultiplier tube (PMT) to enable the detection of moonlit clouds. The boost in gain enables the detection of lights present at the Earth's surface. Most of the lights are from human settlements (cities and towns) and ephemeral fires. Gas flares are also detected and can easily be identified when they are offshore or in isolated areas not impacted by urban lighting.
The National Oceanic and Atmospheric Administration (NOAA) National Geophysical Data Center (NGDC) serves as the long-term archive for DMSP measurements, with data extending from 1992 to the present. The archive is organized as individual orbits which are labeled to indicate the year, month, date, and start time. For this study, individual orbits were processed with automatic algorithms that identify image features (such as lights and clouds) and the quality of the nighttime data. The following criteria were used to identify the best nighttime lights data for compositing:

1. Center half of orbital swath (best geolocation, reduced noise, and sharpest features)
2. No sunlight present
3. No moonlight present
4. No solar glare contamination
5. Cloud-free (based on thermal detection of clouds)
6. No contamination from auroral emissions

Nighttime image data from individual orbits that meet the above criteria are added into a global latitude-longitude grid (Plate Carrée projection) having a resolution of 30 arc sec. This grid cell size is approximately a square kilometer at the equator. The average visible band digital number (DN) is calculated by dividing the sum of DN values by the number of valid observations. Lights from fires are removed based on their high DN values and low frequency of occurrence. A background mask covering areas devoid of lights is used to define the background noise level, which defines a locally variable threshold for zeroing the digital values in grid cells that do not contain light detections. By overlaying data from 2 or more years and applying a contrast stretch it is possible to see changes in lighting over time.
The 2009 NL result for Beijing is presented in Figure 2. NL measurements are acquired globally over several decades with a series of DMSP OLS. In this study, intercalibrated stable NL data in version 4 are used. For reference, the NL extent contour derived from 1994–1995 NL data (called NL9495 hereafter) is overlaid on the 2009 NL image in Figure 2. Including low NL values to sufficiently capture small populated communities, NL9495 is used as a proxy indicator of urban and suburban extent in the Global Rural Urban Mapping Project database (CIESIN et al. 2004; Balk 2009). Although NL9495 is known to be more expansive than the true extent of a given urban or suburban area due to the blooming effects (Elvidge et al. 2004; Small et al. 2005), it is useful as the first demarcation within which a city is amply enclosed. The Beijing change is evident in that the strong NL has expanded even beyond the NL9495 contour limit, especially in the south and in the east of Beijing. While sprawling settlement in Beijing is obvious, the NL in the Beijing center is saturated and consequently the central change is not observable. This limitation can be addressed by multispectral low-light imaging capability of future advanced satellite sensors (Elvidge et al. 2007).

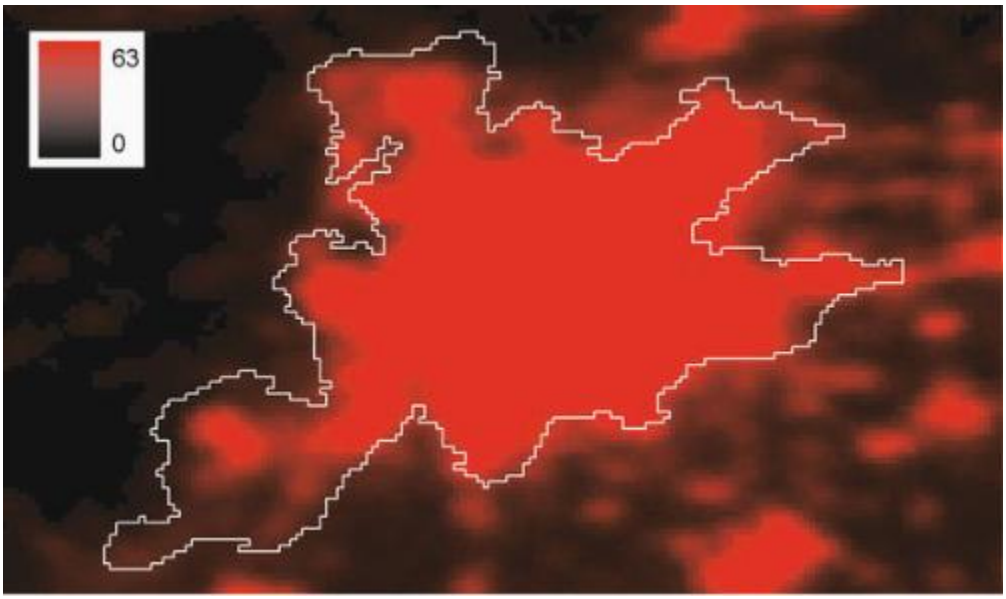

Figure 2 Intercalibrated stable NL of Beijing from F16 DMSP OLS satellite measurements in 2009. The color scale is for NL values from 0 (no light) to 63 (maximum saturated intensity)

Spectral mixing

Landsat provides the basis for spectral mapping of urban and suburban environments, which are characterized by diversity. A diversity of land uses results in a diversity of land cover types and thus a diversity of spectral characteristics. Analysis of laboratory and field spectra of building materials and impervious surfaces confirms both unique spectral absorptions associated with specific, generally synthetic, materials (Herold et al. 2004; Small 2009) and the presence of numerous impervious materials that are spectrally indistinguishable from naturally occurring substrates (Small 2009). In addition to substrates and impervious surfaces, there is also a fundamental ambiguity in the spectral similarity between indigenous and urban vegetation types.

The spectral nonuniqueness of much urban land cover makes it very difficult to accurately delimit urban areas at pixel scales with broadband sensors. Spectral mixing at subpixel scales further complicates the problem. Spatial analysis of high resolution (1 m) panchromatic imagery from a diversity of urban areas worldwide indicates that the characteristic scale of most urban land cover is in the range of 10–20 m (Small 2003, 2009). Consequently, almost all pixels imaged by decameter resolution sensors like Landsat are spectrally mixed pixels. Comparative spectral mixture analysis of Landsat 7 multispectral imagery for 30 cities worldwide indicates that there is no unique spectral signature (or range of signatures) that consistently distinguish urban land cover from a wide variety of nonurban land cover types at pixel scales. However, the spectral heterogeneity of urban land cover can often be used to distinguish it from many nonanthropogenic land cover types that are more spectrally homogeneous at pixel scales.

The accuracy of urban land cover classification depends as much on the surrounding nonurban land cover as it does on the urban area itself. In many temperate and tropical environments urban areas are surrounded by densely vegetated land cover – either indigenous or agriculture. In these cases the urban land cover can often be distinguished by the comparatively low vegetation densities as many urban environments are characterized by little or no vegetation (Small 2005, 2009). In arid and semiarid environments, where undeveloped land covers tend to have a variety of exposed rock and soil substrates similar or identical to local building materials, this distinction is absent and it becomes much more difficult to accurately map urban land cover with decameter scale multispectral imagery (Small 2005).

Despite the pervasive spectral ambiguities, it is often possible to derive bounding estimates of urban extent from multispectral imagery. Because many urban areas are characterized by some consistency in building materials, and the pervasive presence of deep shadow, spectral mixtures of substrate and shadow often distinguish urban environments from vegetated surroundings. Starting with training spectra from unambiguously urban core areas, it is possible to incrementally increase the spectral heterogeneity along a mixing trajectory between shadow and substrate to derive bounding estimates of urban extent. Urban extent can often be bounded by deriving conservative and liberal estimates of

urban land cover and comparison to higher resolution imagery. The difference in location and spatial extent of these estimates is generally small compared to the average size (Small et al. 2005). Figure 3 shows an example of such bounding estimates for Beijing and how they compare to night-light intensity in 2008. The utility of bounding maps like this is in their ability to characterize the location, size, and approximate extent of urban land cover relative to surrounding land covers which might be classified with greater accuracy. The limitation is the potential for considerable spectral ambiguity and pixel scale classification errors of both commission and omission.

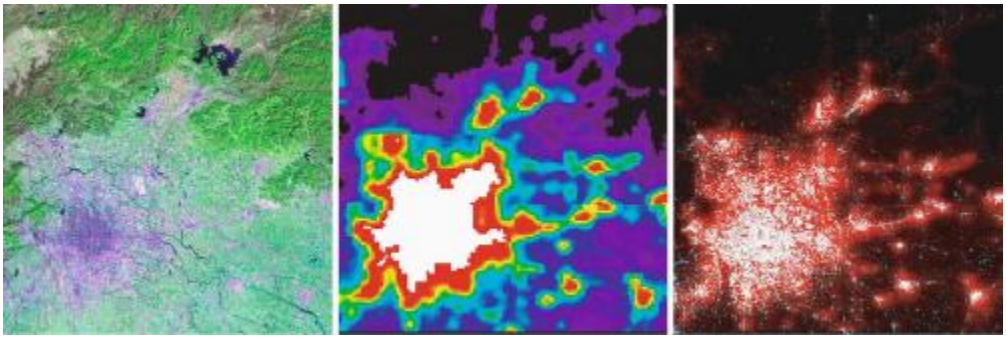

Figure 3 Urban–rural land cover gradients in reflected and emitted light. Landsat 5 false color composite (left) in 2008 shows developed, agricultural, and undeveloped land cover. Homogeneous green areas are agriculture while the dark pink, purple, and gray areas are generally associated with mixtures of SWIR-bright building materials and deep shadow characteristic of more intensive development. Stable night-light brightness (center) for 2008 ranges from dim low DN values (purple to cyan) to brighter (green to red) and saturated (white). Unlighted areas (black) are undeveloped. Day-night composites (right) combine Landsat and night-lights to illustrate consistencies in land cover and night-light brightness. Superimposed night-light brightness (red) on upper (green) and lower (blue) bounding estimates of built-up extent shows high density built environments (white) associated with bright night-lights while agriculture and low density rural land cover are associated with lower light levels (DN < ~20)

Scatterometer

Ku-band backscatter data were obtained globally by the SeaWinds scatterometer on the QuikSCAT (QSCAT) satellite since July 1999 (Jet Propulsion Laboratory 2006). The scatterometer footprint (two-way, half-power, full beamwidth) has an elongated or “egg” shape of about 25 km in azimuth by 37 km in range. Such coarse footprint renders the standard QSCAT data inapplicable to observations of urban areas that require a much higher resolution.

Earlier approaches to increase resolution involve matrix inversion, which is in essence the traditional deconvolution method (DCM). Álvarez-Pérez et al. (2000) assume azimuthally independent radar echo so that DCM can be used; however, the alignment of buildings and man-made structures in cities results in azimuthally dependent backscatter, which violate the validity condition for DCM. DCM further requires that backscatter of the targeted area remains unchanged during the time period of data acquisition for the resolution enhancement (Early and Long 2001). This additional requirement further invalidates the DCM whenever backscatter changes (e.g., by snowmelt, precipitation, flood, diurnal effects, temperature change, etc.).

To account for the DCM shortfall, DSM (Nghiem et al. 2009) is developed to derive backscatter at a resolution much higher than the 25 km by 37 km footprint. In DSM, the Rosette Transform is applied to both the mean and the fluctuating part of backscatter data collocated at each location within each 1-km^2 area. The major advantage is that DSM allows the target to change in azimuth and in time to achieve the high resolution using a composition of data over a long period to minimize speckle in the resultant image (the longer the time period the better). All 10 years of QSCAT data can be used together to obtain DSM σ_0 and IV for decadal observations of urban and suburban environment. Moreover, QSCAT data can be partitioned seasonal, annually, or interannually to monitor urban change at different timescales.

DSM is applied to study Beijing urban characteristics in this study. The DSM σ_0 (Figure 4), derived from QSCAT data acquired in 2009, shows the extensive Beijing sprawl especially in the southeast side well beyond the NL9495 limit. Compared to the NL 2009 (Figure 2), DSM σ_0 detects more sprawling in the southeast extending into Daxing Xian and Tongzhou. Both DSM σ_0 and NL agree that there is less expansion in the north and the west of Beijing where complex mountains hinder the urban growth.

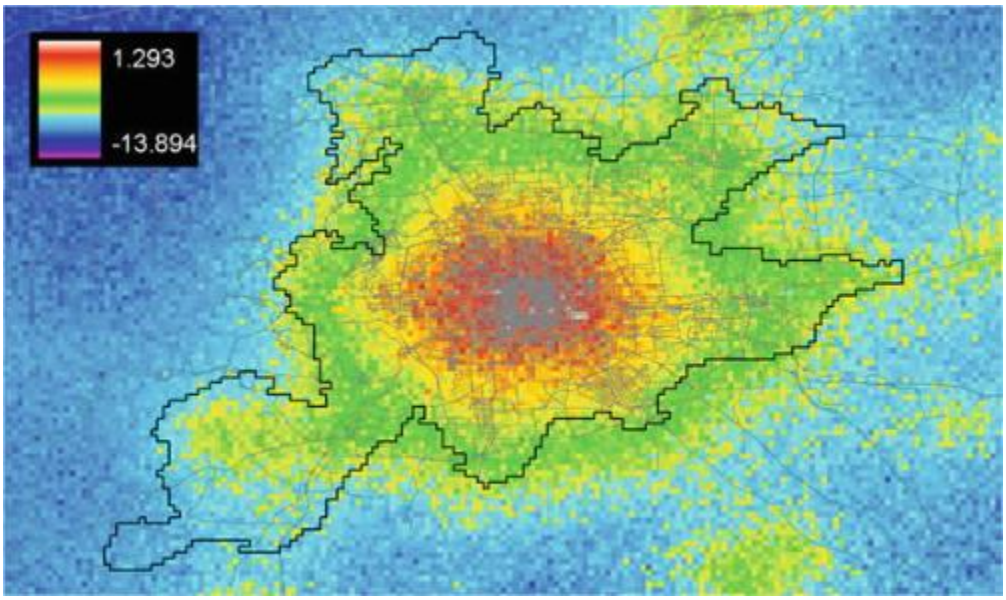

Figure 4 DSM σ_0 of Beijing from QSCAT satellite measurements in 2009. The color scale is for backscatter from low value (magenta) to high value (white). Beijing road network (thin gray lines) is overlaid on the DSM map with road data from CloudMade.com at http://downloads.cloudmade.com (accessed on July 1, 2010). The road data are updated weekly (http://www.openstreetmap.org)

There are small isolated areas identifiable by brighter NL compared to the surroundings (e.g., reddish areas in Daxing Xian and Tongzhou outside the NL9495 limit in the NL image in Figure 2); however, such areas are not distinguished in the DSM σ_0 image (Figure 4). This result suggests that buildings, houses, or other man-made infrastructures, which should have high backscatter, are not substantial in those small communities. This is a limitation of the QSCAT DSM data, and future satellite scatterometers should have a smaller footprint or data should be processed into thinner slices for a higher resolution so that small human settlements can be identified.

More than just the city extent, the DSM σ_0 image in Figure 4 reveals the core of Beijing (orange to red) with a transition (yellow) into the greater Beijing (green). This urban typology is observable by DSM σ_0 because the mean backscatter has a large dynamic range that can account for radar signatures of different urban areas in Beijing without the saturation problem. The Beijing core identified by DSM σ_0 corresponds to the area of high density of roads (Figure 4). Multiple rings of roads in the Beijing road network encircle the city center with the larger rings closer to the outer part of the Beijing core (orange to red area in Figure 4), which characterize the distinct concentric sprawl, a serious violation of the General Plan of Beijing (Shenghe et al. 2002).

Combining remote sensing and demography

Each satellite sensor has certain capabilities and limitations. To achieve an optimal set of information characterizing urban environments, a combination of multisatellite data together with census data is necessary. The integration of remote sensing data from different satellite sensors in a Geographic Information System (GIS) environment represents a well established approach being widely recognized as powerful and efficient in monitoring and evaluating urban sprawl and urban land use and land cover change over a specific period of time (Mesev 1997; Wu et al. 2006; Jat et al. 2008; Feng 2009). Rindfuss et al. (2003), in particular, highlighted the importance of combining remote sensing data with demographic data, primarily from surveys, and identified it as one of the key aspects in urban land use and land cover change studies (also see Liverman et al. 1998).

DSM-processed QSCAT data provide results evenly gridded at 30 arc sec in latitude and in longitude as a rectangular array of points in a Geographic Coordinate System (GCS) – World Geodetic System (WGS) 84 datum. The reference point is at 0° latitude and 0° longitude, and the rectangular array ranges from 0° to [360–(1/120)]° eastward and from 0° to 88° and −88° northward and southward, respectively. With each point storing its own geographic coordinates, each DSM σ_0 and the associated IV value can be referred to the area (approximately a square kilometer at the equator) it

represents. Thus, the rectangular array of points can be used to create a raster grid, with a pixel size of 30 arc sec, in which each cell is identified by the values stored in the point located at its southwest corner (Nghiem et al. 2009).

Each QSCAT raster grid from 2000 to 2009 is coregistered (i.e., spatially aligned so that all pixels representing the same area and location in different rasters are exactly coincidental) with the DMSP-OLS NL raster dataset and with two different population raster datasets modeling the global residential (P_r) and ambient (P_a) population distribution, in order to run a pixel-by-pixel analysis in a GIS environment. Both the Global Rural Urban Mapping Project (GRUMP) dataset representing P_r (CIESIN et al. 2004) and the LandScan^{TM} (LandScan 2008^{TM}/UT-Battelle, LLC) dataset representing P_a (Dobson et al. 2000) depict the distribution of human population across the globe at a resolution of 30 arc sec. These datasets result from methods that transform population data from their native irregularly shaped spatial units (vector format), which are usually administrative and of varying shape, size, and resolution, to a regular raster grid of quadrilateral latitude–longitude cells at a fixed resolution (Tobler et al. 1997; Deichmann et al. 2001; Dobson et al. 2003; Balk and Yetman 2005). In particular, the allocation mechanism for GRUMP P_r explicitly takes into account population and extent of urban areas (see Balk et al. 2006; Balk 2009, for a detailed description of the methodology), whereas the allocation mechanism for LS P_a is based on likelihood coefficients calculated considering multiple key indicators of population distribution (see Oak Ridge National Laboratory, 2010, for a description of the general methodology).

In this study, GIS technology is used to process and combine different remote sensing products in order to characterize the Beijing environment in the decade of 2000s (2000–2009) and to highlight the relationship between the remote sensed "urban sprawl indicators" (NL and QSCAT DSM datasets) and the distribution of the population (as represented both in the GRUMP and in the LS datasets) in the Beijing urban and suburban area. We present the linear correlation results, between the two population raster datasets and both DSM and NL values (Table 1), for Beijing urban and suburban area within the common NL9495 extent. Both the DSM and the NL values used in the analysis were averaged between 2000 and 2009 while the GRUMP and the LS datasets depict, respectively, P_r in the 2000 and P_a averaged over 2004, 2006, 2007, and 2008. Due to the large number of raster grid cells, and because a relatively high number of observations would render even very weak relationships as significant, we use a 5% random sample of those cells to obtain an appropriate representation of the relationships.

Table 1 Correlation analysis between population data (GRUMP 2000 and LS 2004–2008) and remote sensing signatures (DSM backscatter and NL brightness)

Urban area	n (5% cases)	GRUMP 2000		LS 2004–2008	
		DSM 00-09	NL 00-09	DSM 00-09	NL 00-09
Beijing	248	−0.046	−0.12	0.724	0.475

Results from the correlation analysis in Table 1 show a very small correlation coefficient between either DSM σ_0 or NL and P_r from GRUMP 2000. Since infrastructures represented by DSM σ_0 and anthropogenic lights represented by NL must be both physically related to human settlements, the weak negative correlation suggests that P_r is not colocated in the dense built-up areas. In contrast, a strong association is found between DSM σ_0 and P_a from LandScan^{TM} (LS) because houses, offices, factories or other infrastructures are where people are most likely to be located physically at any time. Similarly, there is an association between NL and P_a. The strong σ_0–P_a relationship supports the use of radar data in demography and socioeconomic science.

Figure 5 illustrates the composite approach combining both remote sensing and demographic data to observe urban characteristics of Beijing. The DSM σ_0, averaged over all data collected in 2000–2009, represents the urban extent and typology in the decade of 2000s. In Figure 5, the spatial pattern of DSM time-average backscatter and that of the LS P_a are similar and thus explain the high correlation between the scatterometer remote sensing data and the ambient population census, whereas the residential population P_r, which is partitioned into each administrative unit, has a spatial distribution different from the scatterometer observation. Larger values (green-yellow, top right panel in Figure 5) of the DSM IV indicate that large changes have occurred in the central core and also in the transition areas of Beijing. The NL image, from data averaged over 2000–2009, has less spatial distinction compared to that of the DSM backscatter within the NL9495; however, NL can detect many more small settlements outside the NL9495 contour. In contrast to both DSM and NL results, Landsat data reveal a much higher resolution containing more spatial details.

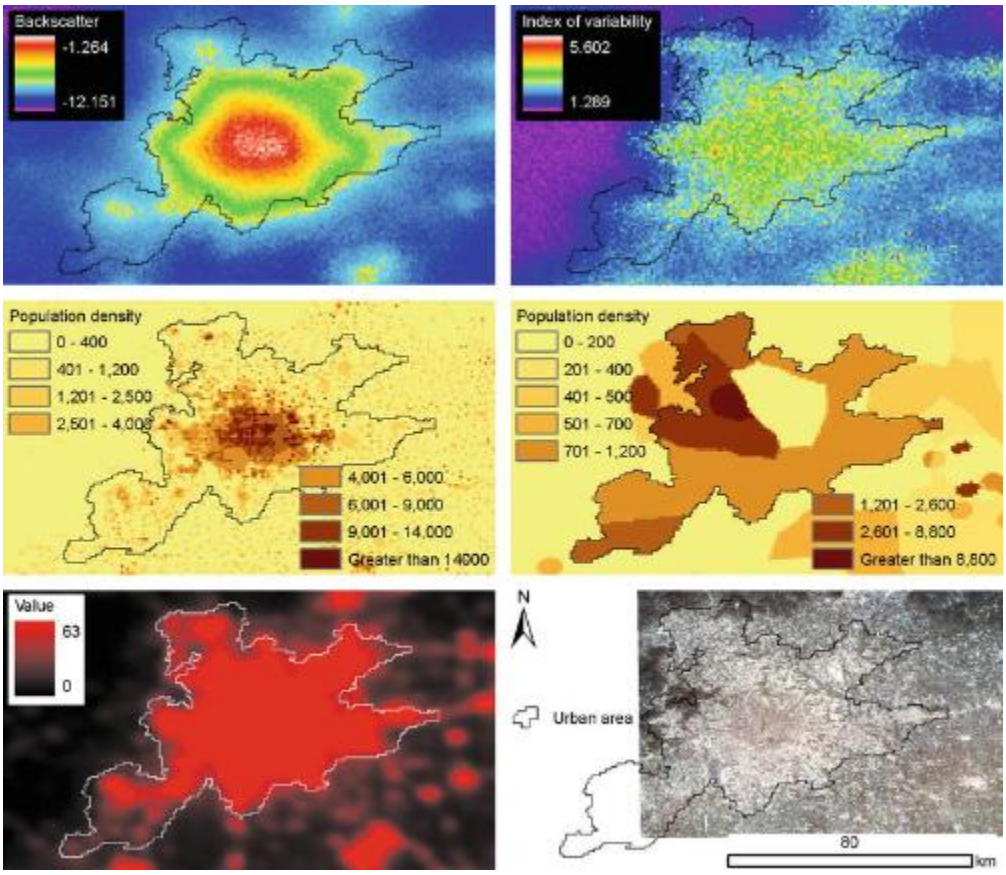

Figure 5 Composite results for Beijing: Top left panel for 2000–2009 DSM average backscatter, top right panel for 2000–2009 DSM IV, middle left panel for average ambient population P_a from LS 2004–2008, middle right panel for residential P_r from GRUMP 2000, bottom left panel for 2000–2009 NL, and bottom right panel for Landsat. NL9495 contour is overlaid on all images as the common reference area

Summary

Various remote sensing methods and demographic datasets are used in the Beijing case study to illustrate their capability to observed physical and demographic characteristics of the urban environment. NL data serve well to identify the outer limit of not only large urban areas but also small settlements. For each large urban contour limit from NL, DSM scatterometer data can detect urban extent and typology. Within each urban type classified by DSM data, Landsat spectral signatures can provide high-resolution details of the urban land cover. It is found that DSM σ_0 has the highest correlation with ambient population of Beijing. To monitor urban change, data can be partitioned into different timescales. The combination of multiple remote sensing methods together with demographic measures is necessary to effectively observe urban environments, rather than each dataset standing alone – both by adding shape and contour to urban population estimates as well as to describe patterns of association between population models and those detecting the rapidly changing built-environment. Although Beijing may have local characteristics in detail, it shares many issues of a megacity common to other megacities across the world, where methods and results in this Beijing study can be applicable.

While several important remote sensing approaches applicable to global urban observations are presented here, this Beijing case study is by no means exhaustive. Global synthetic aperture radar (SAR) data such as from the Space Shuttle Radar Mission (STRM) has a great potential to obtain a uniform database of global infrastructure representing the state of global urban environments in the specific period of data collection (Nghiem et al. 2001). With the interferometric SAR capability, the recent TanDEM-X Mission (Krieger et al. 2010) and the future DESDynI Mission (National Research Council 2007) can provide three-dimensional data to measure building height, while a future class of optical sensors such

as that proposed for the Nightsat Mission (Elvidge et al. 2007) can significantly improve the urban remote sensing capability. These advances are critical for developing a consistent global urban infrastructure dataset to meet the need of the social and physical scientific communities as well as policy and decision makers.

Cross-references

Data Archival and Distribution
Microwave Radiometers
Optical/Infrared Sensors
Radar
Scattering

Acknowledgments

The research carried out at the Jet Propulsion Laboratory (JPL), California Institute of Technology, was supported under a contract with the National Aeronautics and Space Administration (NASA) Land-Cover and Land-Use Change (LCLUC) Program. The DSM development was funded through the Director's Research and Development Fund (DRDF) program at JPL.

Bibliography

- Álvarez-Pérez, J. L., Marshall, S. J., and Gregson, K., 2000. Resolution improvement of ERS scatterometer data over land by Wiener filtering. Remote Sensing of Environment, 71, 261–271.
- Angel, S., Parent, J., and Civco, D., 2007. Urban sprawl metrics: an analysis of global urban expansion using GIS. In ASPRS Annual Conference, Tampa, Florida.
- Balk, D., Pozzi, F., Yetman, G., Deichmann, U., and Nelson, A., 2005. The distribution of people and the dimension of place: methodologies to improve the global estimation of urban extents. In Proceedings of the Urban Remote Sensing Conference. Tempe, AZ: International Society for Photogrammetry and Remote Sensing.
- Balk, D., and Yetman, G., 2005. The global distribution of population: Evaluating the gains in resolution refinement. Available from World Wide Web: http://beta.sedac.ciesin.columbia.edu/gpw/docs/gpw3_documentation_ final.pdf (accessed June 22, 2010).
- Balk, D., Deichmann, U., Yetman, G., Pozzi, F., Hay, S. I., and Nelson, A., 2006. Determining global population distribution: Methods, applications and data. In Hay, S. I., Graham, A. J., and Rogers, D. J. (eds.), Global Mapping of Infectious Diseases: Methods, Examples and Emerging Applications. London: Academic. Advances in Parasitology, Vol. 62, pp. 119–156.
- Balk, D., 2009. More than a name: why is global urban population mapping a GRUMPy proposition? In Gamba, P., and Herold, M. (eds.), Global Mapping of Human Settlement: Experiences, Data Sets, and Prospects. New York: Taylor and Francis, pp. 145–161.
- Chengrong, D., Ge, Y., Fei, Z., Xuehe, L., 2008. Nine trends of changes of China's floating population since the adoption of the reform and opening-up policy, China Population Today, 25(4).
- CIESIN (Center for International Earth Science Information Network) of Columbia University. International Food Policy Research Institute (IPFRI), the World Bank, and Centro Internacional de Agricultura Tropical (CIAT), 2004. Global rural–urban mapping project (GRUMP). Urban extents. alpha version. Palisades, NY, CIESIN, Columbia University. http://sedac.ciesin.columbia.edu/gpw/documentation.jsp (accessed June 22, 2010).
- Deichmann, U., Balk, D., and Yetman, G., 2001. Transforming population data for interdisciplinary usages: from census to grid. Available from World Wide Web: http://sedac.ciesin.columbia.edu/gpw-v2/GPWdocumentation.pdf (accessed June 22, 2010).
- Dobson, J. E., Bright, E. A., Coleman, P. R., Durfee, R. C., and Worley, B. A., 2000. A global population database for estimating populations at risk. Photogrammetric Engineering and Remote Sensing, 66(7), 849–857.
- Dobson, J. E., Bright, E. A., Coleman, P. R., and Bhaduri, B. L., 2003. LandScan: a global population database for estimating populations at risk. In Mesev, V. (ed.), Remotely Sensed Cities. London: Taylor & Francis, pp. 267–281.
- Early, D. S., and Long, D. G., 2001. Image reconstruction and enhanced resolution imaging from irregular samples. IEEE Transactions on Geoscience and Remote Sensing, 39, 291–302.
- Elvidge, C. D., Baugh, K. E., Kihn, E. A., Kroehl, H. W., and Davis, E. R., 1997. Mapping city lights with nighttime data from the DMSP operational linescan system. Photogrammetric Engineering and Remote Sensing, 63, 727–734.
- Elvidge, C. D., Imhoff, M. L., Baugh, K. E., Hobson, V. R., Nelson, I., Safran, J., Deitz, J. B., and Tuttle, B. T., 2001. Night-time lights of the world: 1994–1995. ISPRS Journal of Photogrammetry and Remote Sensing, 56(2), 81–99.
- Elvidge, C. D., Safran, J., Nelson, I. L., Tuttle, B. T., Hobson, V. R., Baugh, K. E., et al., 2004. Area and position accuracy of DMSP nighttime lights data. In Lunetta, R. S., and Lyon, J. G. (eds.), Remote Sensing and GIS Accuracy Assessment. Boca Raton, FL: CRC Press, pp. 281–292.
- Elvidge, C. D., Cinzano, P., Pettit, D. R., Arvesen, J., Sutton, P., Small, C., Nemanis, R., Longcore, T., Rich, C., Safran, J., Weeks, J., and Ebener, S., 2007. The Nightsat mission concept. International Journal of Remote Sensing, 28(12), 2645–2670.
- Feng, L., 2009. Applying remote sensing and GIS on monitoring and measuring urban sprawl. A case study of China. Revista Internacional Sostenibilidad, Tecnología y Humanismo, 4, 47–56.
- Herold, M., Roberts, D. A., Gardner, M. E., and Dennison, P. E., 2004. Spectrometry for urban area remote sensing – development and analysis of a spectral library from 350 to 2400 nm. Remote Sensing of Environment,

91, 304–319.

- Jat, M. K., Garg, P. K., and Khare, D., 2008. Monitoring and modelling of urban sprawl using remote sensing and GIS techniques. International Journal of Applied Earth Observation and Geoinformation, 10(1), 26–43, doi:10.1016/j.jag.2007.04.002.
- Jet Propulsion Laboratory, 2006. QuikSCAT Science Data Product User's Manual. Jet Propulsion Laboratory Document D-18053-RevA. Pasadena, CA: JPL.
- Krieger, G., Hajnsek, I., Papathanassiou, K. P., Younis, M., and Moreira, A., 2010. Interferometric synthetic aperture radar (SAR) missions employing formation flying. Proceedings of the IEEE, 98(5), 816–843.
- Liu, S., Prieler, S., and Li, X., 2002. Spatial patterns of urban land use growth in Beijing. Journal of Geographical Sciences, 12(3), 266–274.
- Liverman, D., Moran, E., Rindfuss, R., and Stern, P., 1998. People and Pixels: Linking Remote Sensing and Social Science. Washington, DC: National Academy Press.
- Mesev, V., 1997. Remote sensing of urban systems: Hierarchical integration with GIS. Computers, Environment and Urban Systems, 21(3/4), 175–187.
- National Research Council, 2007. Earth Science and Applications from Space: National Imperatives for the Next Decade and Beyond. Washington, D.C: The National Academies Press.
- Nghiem, S. V., Balk, D., Small, C., Deichmann, U., Wannebo, A., Blom, R., Sutton, P., Yetman, G., Chen, R., Rodriguez, E., Houshmand, B., and Neumann, G., 2001. Global Infrastructure: The Potential of SRTM Data to Break New Ground, a white paper of the Global Infrastructure Mapping Workshop, JPL D-23049, Pasadena, CA: Jet Propulsion Laboratory, California Institute of Technology, 22 pp.
- Nghiem, S. V., Balk, D., Rodriguez, E., Neumann, G., Sorichetta, A., Small, C., and Elvidge, C. D., 2009. Observations of urban and suburban environments with global satellite scatterometer data. ISPRS Journal of Photogrammetry and Remote Sensing, 64, 367–380, doi:10.1016/j.isprsjprs.2009.01.004.
- Oak Ridge National Laboratory, 2010. LandScanTM Global Population Database, Oak Ridge National Laboratory, Geographic Information Science and Technology (GIST) Group, Oak Ridge, Tennessee. Available from World Wide Web: http://www.ornl.gov/sci/landscan/landscan_documentation.shtml (accessed July 29, 2010).
- Owen, T. W., Gallo, K. P., Elvidge, C. D., and Baugh, K. E., 1998. Using DMSP-OLS light frequency data to categorize urban environments associated with US climate observing stations. International Journal of Remote Sensing, 19, 3451–3456.
- Rindfuss, R., Walsh, S., Mishra, V., Fox, J., and Dolcemacolo, G., 2003. Linking household and remotely sensed data: methodological and practical problems. In Fox, J., Rindfuss, R. R., Walsh, S. J., and Mishra, V. (eds.), People and the environment: approaches for linking household and community surveys to remote sensing. Boston, MA: Kluwer, pp. 1–29.
- Shenghe, L., Prieler, S., and Xiubin, L., 2002. Spatial patterns of urban land use growth in Beijing. Journal of Geographical Sciences, 12(3), 266–274.
- Small, C., 2003. High resolution spectral mixture analysis of urban reflectance. Remote Sensing of Environment, 88, 170–186.
- Small, C., 2005. Global analysis of urban reflectance. International Journal of Remote Sensing, 26(4), 661–681.
- Small, C., Pozzi, F., and Elvidge, C. D., 2005. Spatial analysis of global urban extent from DMSP-OLS night lights. Remote Sensing of Environment, 96(3–4), 277–291.
- Small, C., 2009. The color of cities: an overview of urban spectral diversity (Invited chapter). In Herold, M., and Gamba, P. (eds.), Global Mapping of Human Settlements. London: Taylor & Francis.
- Sutton, P., Roberts, C., Elvidge, C., and Meij, H., 1997. A comparison of nighttime satellite imagery and population density for the continental United States. Photogrammetric Engineering and Remote Sensing, 63, 1303–1313.
- Sutton, P., Roberts, D., Elvidge, C., and Baugh, K., 2001. Census from Heaven: an estimate of the global human population using night-time satellite imagery. International Journal of Remote Sensing, 22, 3061–3076.
- Tobler, W., Deichmann, U., Gottsegen, J., and Maloy, K., 1997. World population in a grid of spherical quadrilaterals. International Journal of Population Geography, 3(3), 203–225.
- Wu, Q., Li, H., Wang, R., Paulussen, J., He, Y., Wang, M., Wang, B., and Wang, Z., 2006. Monitoring and predicting land use change in Beijing using remote sensing and GIS. Landscape and Urban Planning, 78(4), 322–333, doi:10.1016/j.landurbplan.2005.10.002.
- Yeh, A. G. O., and Xu, J., 2009. China's post-reform urbanization: Trends and policies, International Institute for

Environment and Development (IIED) – UNFPA Workshop on Population and Urbanization Issues, London, UK.

Remote Sensing of Urban Environments - the Beijing Case Study

Dr. Son V. Nghiem	Jet Propulsion Laboratory, Pasadena, USA
Dr. Alessandro Sorichetta	Dipartimento di Scienze della Terra “A. Desio”, Università degli Studi di Milano, Milan, Italy
Dr. Chris Elvidge	Earth Observation Group, NOAA-NESDIS National Geophysical Data Center E/GC2, Boulder, USA
Dr. C. Small	Lamont Doherty Earth Observatory, Marine Geology and Geophysics, Columbia University, Palisades, USA
Dr. Deborah Balk	School of Public Affairs, Baruch College, City University of New York, New York, USA
Dr. U. Deichmann	Development Research Group, The World Bank, Washington DC, USA
Dr. Gregory Neumann	Jet Propulsion Laboratory, California Institute of Technology, Pasadena, USA

DOI:	10.1007/SpringerReference_327195
URL:	http://www.springerreference.com/index/chapterdbid/327195
Part of:	Encyclopedia of Remote Sensing
Editor:	Dr. Eni G. Njoku
PDF created on:	November, 28, 2012 16:57